Mesoscale studies of ionic closed membranes with polyhedral geometries

Monica Olvera de la Cruz[a]
Department of Materials Science and Engineering, Northwestern University, Evanston, Illinois 60208, USA; Department of Physics and Astronomy, Northwestern University, Evanston, Illinois 60208, USA; and Department of Chemistry, Northwestern University, Evanston, Illinois 60208, USA

(Received 10 February 2016; accepted 23 May 2016; published online 10 June 2016)

Large crystalline molecular shells buckle spontaneously into icosahedra while multicomponent shells buckle into various polyhedra. Continuum elastic theory explains the buckling of closed shells with one elastic component into icosahedra. A generalized elastic model, on the other hand, describes the spontaneous buckling of inhomogeneous shells into regular and irregular polyhedra. By co-assembling water-insoluble anionic (−1) amphiphiles with cationic (3+) amphiphiles, we realized ionic vesicles. Results revealed that surface crystalline domains and the unusual shell shapes observed arise from the competition of ionic correlations with charge-regulation. We explain here the mechanism by which these ionic membranes generate a mechanically heterogeneous vesicle.
[http://dx.doi.org/10.1063/1.4953570]

Convex polyhedral shells have been observed in various microscopic systems including viral capsids,[1] fullerenes,[2] protein-based bacterial organelles,[3] and co-assembled ionic amphiphiles.[4] The most commonly observed polyhedral symmetry in self-organized homogeneous structures is the icosahedron, which has the highest possible symmetry. We explain here a way to design various polyhedral shapes with reduced symmetry using elasticity theory[5] and full atom and coarse-grained computer simulations with input from experimental studies.[4]

Elasticity theory[6] explains that the lowest-energy configuration of a buckled crystalline shell is an icosahedron.[7] The theory describes how any spherical crystalline shell made of a homogenous, isotropic, elastic material *buckles* into an icosahedron when the Föppl–von Kármán number $\gamma = YR^2/\kappa$, where Y is the Young's modulus, κ is the bending rigidity, and R is the linear size of the shell, is sufficiently high. Since closed crystalline membranes have at least 12 five-fold disclinations that repeal each other, these defects are positioned at the vertices of an inscribed icosahedron in the sphere.[8] When the Föppl–von Kármán number exceeds a critical value, these defects buckle simultaneously, and the spherical shell acquires an icosahedral shape.

Recently, we found that elastic membranes with elastic heterogeneities, which are achieved via increasing the number of the shell components, buckle into regular and irregular polyhedra, as shown in Figure 1.[5] We analyzed the simplest case of a two-dimensional membrane composed of *two* components A and B that are individually isotropic and characterized by their Young's modulus, Y_A, Y_B, and bending rigidity κ_A, κ_B; the Poisson ratios were set equal to $\nu_A = \nu_B \sim 0.33$. We found the lowest energy-state configuration by discretizing a model for elastic membranes.[9] The Hamiltonian is given by the sum of two contributions, the bending energy E_b, and the elastic E_s energy given. The bending energy is

Note: Invited for the Materials Genome special topic.

[a]Author to whom correspondence should be addressed. Electronic mail: m-olvera@northwestern.edu

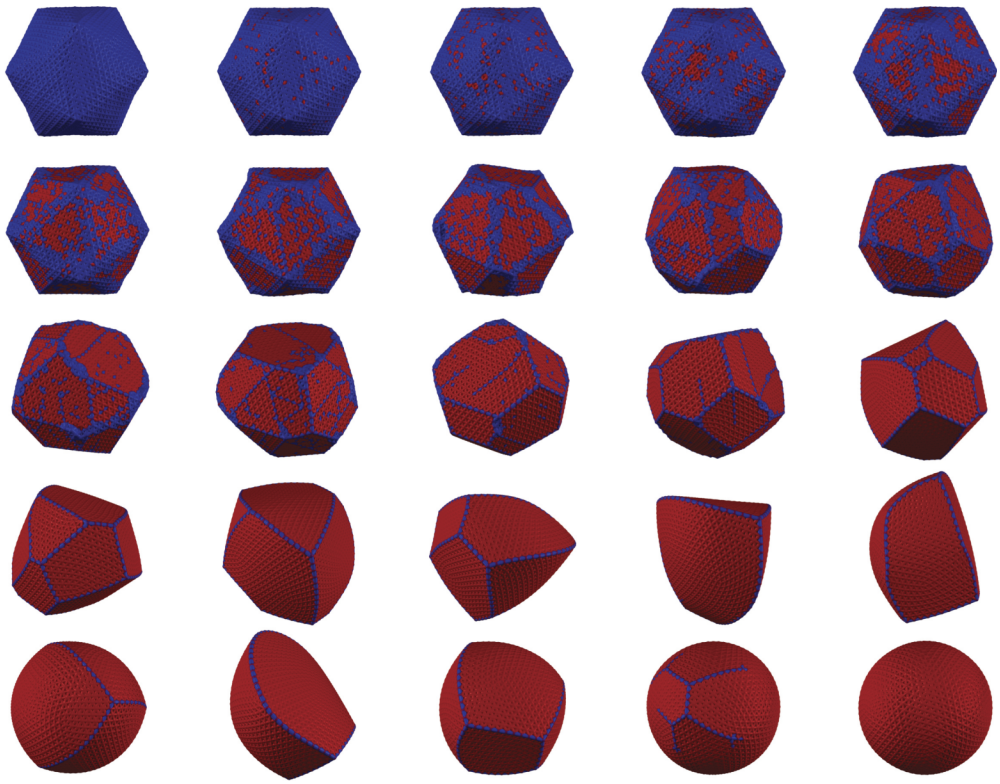

FIG. 1. Snapshots of configurations at different fraction f. The A-component (in blue) has $Y_A = 5.77$ and $\kappa_A = 0.06$ while the B-component (in red) has $Y_B = 5.77$ and $\kappa_B = 28.9$. The radius of the shell is about R ~ 11.3 in units of the average bond length. The fraction f varies (from left to right, top to bottom) as f = 0%, 4%, 10%, 20%, 30%, 40%, 50%, 60%, 65%, 70%, 75%, 80%, 85%, 90%, 95%, 95.5%, 96%, 96.5%, 97%, 97.5%, 97.7%, 98%, 98.5%, 99%, 100%. Adapted with permission from Vernizzi *et al.*, Proc. Natl. Acad. Sci. U. S. A. **108**(11), 4292 (2011). Copyright 2011 National Academy of Sciences, USA.

$$E_b = \int dS \left[2\kappa(r)(H - H_0)^2 + \kappa_G(r)G\right],$$

where H is the mean curvature, and G is the Gaussian curvature, and the bending (κ) and Gauss (κ_G) rigidities are a function of the position in the shell surface $r(s_1, s_2)$. The elastic energy is

$$E_s = \frac{1}{2}\int dS \left[\lambda(\mathrm{Tr}\,(u))^2 + 2\mu \mathrm{Tr}\left(u^2\right)\right],$$

where λ, μ are the position dependent Lamé coefficients (for each component, $\lambda_I = \mu_I = Y_I 3/8$, where Y is the Young modulus of component I = A, B). The lowest energy configuration was obtained by Monte Carlo simulated annealing simulations for a fixed relative fraction f of the two components.

Possible buckled structures can be obtained considering components A, B with intermediate compositions f of the B component such that the stable shape in the limits of homogeneous composition is icosahedral ($f = 0$) or spherical ($f = 1$), respectively. A sufficient condition for that to happen is to choose $\kappa_B > \kappa_A$ such that $\gamma_B < \gamma^* < \gamma_A$, where $\gamma_A = Y_A R^2/\kappa_A$ and $\gamma_B = Y_B R^2/\kappa_B$. We considered the B-component more rigid than the A-component ($\kappa_B > \kappa_A$).

At intermediate values of the composition f, the component with low-bending rigidity tends to form lines that merge into vertices. The pattern of lines aids the faceting of the shell into a polyhedral structure often with three-fold vertices. Such vertices are joined together by sharp edges occupied by component A that surrounds polygons. Even though the components are chemically compatible,

they segregate due to their different elastic properties. This can be rationalized using geometric arguments.[10] The Gauss-Bonnet theorem states that the integral of the Gaussian curvature is

$$\int_D dSG + \int_{\partial D} dlk_g = 2\pi\chi_D,$$

where D is the integral over the domain, ∂D is the domain boundary, k_g is the geodesic curvature, and χ_D is the Euler characteristic of the surface. Therefore, applying this theorem to the non-homogenous closed shell with soft and hard domains, one obtains that the Gaussian contribution to the energy is,[10]

$$E_b^G = -\left(\kappa_G^{soft} - \kappa_G^{hard}\right)\int_{\partial D_{soft}} dlk_g + 2\pi\left(\kappa_G^{soft} - \kappa_G^{hard}\right)\chi_{soft},$$

where we used the identity that equates the sum of the Euler characteristics of the soft and hard domains to the Euler characteristic of a closed surface, which is two ($\chi_{soft} + \chi_{hard} = \chi_D = 2$) and also that $\partial D_{hard} = -\partial D_{soft}$, since the boundary of the soft component is the boundary of the hard component but in the opposite direction. Given that in the discretized model[9] used to generate Figure 1, the Gaussian rigidity and the bending rigidity are related by $\kappa_G^I = -2\kappa^I$ for both hard and soft components (I = soft, hard) we obtain,

$$E_b^G = 2\left(\kappa^{soft} - \kappa^{hard}\right)\int_{\partial D_{soft}} dlk_g - 4\pi\left(\kappa^{soft} - \kappa^{hard}\right)\chi_{soft}.$$

Since $\kappa^{hard} > \kappa^{soft}$, both terms favor a large negative ∂D_{soft}, and a large positive integral geodesic curvature of the boundary. This means that a soft-component domain tends to have several boundaries, $\chi_{soft} = 2 - h$, where h is the number of boundaries for a connected domain, and to be negative, h should be at least three. We note that the Euler characteristic of a disk is one. Consequently, the hard-component domain tends to fragment in several disconnected domains, roughly h in number, each one with the topology of a disk.

The Gauss-Bonnet theorem stresses the numerical results that show the buckling in the case of mechanically heterogeneous shells is not mediated by defects, as in the case of homogenous crystalline shells. That is, even if the Hamiltonian for the heterogeneous shells is discretized using a triangular mesh with fixed connectivity and with the required 12 five-fold disclinations, those defects are located in the flat regions of the shell (and are slightly sunken in). The buckling into polyhedra occurs by segregation of the component with lowest bending rigidity into narrow bands that fold; that is, by concentrating the curvature, which is a mechanism that also describes the crumpling of membranes.[11]

We note that in the numerical model, polyhedral structures are expected only in specific regions of the parameter space of the two-component system (R, Y_A, $\kappa_A Y_B$, κ_B). Shape competition between the elastic components is required for buckling into polyhedral shells. Faceting in a shell with a given radius occurs when at least one of the components has a large bending rigidity and a low Young's modulus. For very small shells, however, an exceedingly high Young's modulus and a very low bending rigidity are required. Therefore, faceting effects are expected to occur for a narrow range of shell sizes where the shape-competition is consistent with the elastic parameters of soft materials (at least one component would have to have either extremely large or extremely low Y-to-κ ratio).

Regardless of the apparently highly narrow range of parameter space required for the realization of the buckling of mechanically heterogeneous elastic shells into polyhedra, the model is very robust. As discussed above, the Gauss-Bonnet theorem supports fragmentation of the shells driven by the formation of ridges by the component of lowest bending rigidity. The formation of ridges in the buckling of membranes has long been established.[12] Therefore, it is not surprising that such effect escapes closed membranes' buckling when the folding is facilitated (i.e., by adding a second component that can segregate into ridges). Moreover, it has been shown that faceted bilayer vesicles that allow the segregation of excess amphiphiles along the ridges of polyhedra do have lower bending energies than spherical bilayer vesicles.[13] Therefore, the required ingredients for buckling into polyhedral shells are realizable. Indeed, experiments on bilayers of co-assembled

cationic and anionic amphiphiles revealed giant icosahedral vesicles.[14] These giant icosahedra have pores at the 12 vertices of the faceted vesicles and are only formed at zero salt conditions when there is an excess of an amphiphile component, which segregates at the opening of the pores.

We recently demonstrated the buckling into various polyhedra without pores by co-assembling amphiphiles with various degrees of ionization into ionic vesicles.[4] We generated crystalline membranes in a large variety of geometries, including faceted polyhedral shells by co-assembling cationic (+3) and anionic (−1) amphiphiles at different pH values. Although single-tailed amphiphiles typically form micelles in aqueous solutions, co-assembled cationic-anionic mixtures can form bilayers.[15] In fact, work with polymerizable amphiphiles[16] showed that a large charge imbalance between the cationic and anionic head groups enables their co-assembly into nanoscale buckled vesicles. By co-assembling oppositely charged surfactants without a polymerizable group, we demonstrated that electrostatics drives the crystallization of the tails and determines the crystalline structure of the domains resulting into buckled nanoscale vesicles that are stable at high salt concentrations.[4] The crystalline domains, controlled by pH, lead to the formation of shapes other than icosahedra, very similar to the shapes obtained in the polymerized co-assembled vesicles.[16] These shapes resemble organelle microcompartment geometries[3] and the faceted shape of halophilic organisms.[17]

The selected 3+ cation C_{16}–K_3 dissolves in water and forms micelles of ∼10 nm diameter. However, it can be co-assembled with water-insoluble palmitic acid C_{16}–COOH at different pH values. The TEM images of the cation/anion mixture of amphiphiles show a pH dependent diversity of shapes including faceted vesicles and ribbons.[4] Collected *in situ* small angle x-ray (SAXS) and wide angle x-ray (WAXS) data demonstrated that the structures were consistent with a bilayer crystalline membrane morphology. The WAXS data showed for pH < 7 and pH > 10, the appearance of a single diffraction peak, which indicates that the molecules are packed in a 2D hexagonal lattice; whereas the presence of two diffraction peaks for pH 8–9 indicates a rectangular-C structure. Vesicle shapes were observed by TEM at pH 5 and pH 10 while at pH 8, nanoribbons and sheets were observed. These experimental results demonstrated that changes on the mesoscale structure are due to the nanoscale packing of the molecules.

Monte Carlo simulations were used to determine how pH relates to the degree of ionization of the molecules.[18] Here we summarize the main results of the Monte Carlo simulations of a charge-fluctuating model that treats charge correlations in detail. The degree of dissociation of a lipid bilayer depends on both the salt concentration and the pH value. If the surface is acidic, that is a dissociated head group has a negative charge, at low pH, the excess H^+ ions in the solution will inhibit the dissociation and the bilayer will be essentially neutral.[19] As the pH increases, the dissociation becomes more favorable and the surface gradually becomes charged. When pH is equal to the pK_a of a given molecule, on average 50% of the head groups are dissociated. When interactions between charges on the bilayer surface are included, the electrostatic repulsion between two negative charges will inhibit the dissociation. Meanwhile, when a positive charge is next to the negative charge, the average dissociation rate will be enhanced.

We modeled the effects of electrostatic interactions via a discrete, lattice model introduced by Netz.[18] We constructed an appropriate lattice with lattice constant $a = 1$, that is, use the lattice spacing as the unit of length. In our particular experimental system of interest, a roughly corresponds to 0.5 nm. The Hamiltonian is given by

$$\frac{H}{k_BT} = \frac{\mu_A}{k_BT}\sum_i n_i^A + \frac{\mu_B}{k_BT}\sum_i n_i^B + \frac{1}{2}\sum_{i,j}(-1)^{\eta_{ij}} l_B \frac{e^{-r_{ij}/\zeta}}{r_{ij}},$$

where $\eta_{ij} = 0$ (1) if sites i and j are of the same (different) type and $n_i^{A(B)} = 0$ or 1 is the dissociation state of the acidic (basic) site i. The Debye screening length is given by $\zeta = 1/(4\pi\, l_B \sum z_i^2 c_i)^{1/2}$, where z_i and c_i and valence and the concentration of salt ions, and the Bjerrum length, $l_B = e^2/4\pi\varepsilon_0\varepsilon_r k_B T$, is the length at which electrostatic interaction is comparable with thermal energy k_BT, where e is the unit charge, ε_r is the relative permittivity of the medium, and ε_0 is the dielectric

permittivity of vacuum. The chemical potentials are given by

$$\frac{\mu_A}{k_BT} = -\ln 10\left(pH - pKa_{(A)}\right)$$
$$\frac{\mu_B}{k_BT} = \ln 10\left(pH - pKa_{(B)}\right)$$

Monte Carlo simulations were used to determine the average dissociation fraction of the co-assembled system as a function of pH and Debye screening length ζ. While the charge dissociation for single-component systems is heavily suppressed by the electrostatic repulsion between neighboring sites (ideal case), in the case of mixtures, the dissociation is favorable and the system is completely charged over a range of pH values.

Molecular dynamics (MD) simulations were performed at a low degree of ionization of the palmitic acid groups to mimic the low pH data and a high degree of ionization to explain the high pH data. The atomistic simulations were carried out for electroneutral systems with 30% (Figure 2(a)) and 95% (Figure 2(b)) average ionization of the palmitic acid molecules, which correspond roughly to pH 4 and 8, respectively. Interdigitation of the upper and the lower layer in the bilayer was observed only in the system with 95% ionization of palmitic acid. The rectangular-C packing of the tails observed experimentally was not reproduced by the MD simulations. This is possibly due to the force fields, which were not parameterized for crystalline phases.

A simple estimate of the electrostatic correlations can explain the formation of the crystalline phase in the vesicles. The head groups located between polar water ($\varepsilon_r \approx 80$) and nonpolar tails ($\varepsilon_r \approx 1$) experience a dielectric response of the order of the mean between the two media, $\varepsilon_r \approx 40$, resulting in $l_B \; e^2/4\pi\varepsilon_0\varepsilon_r k_BT \approx 1.4$ nm. The electrostatic energy to hold together

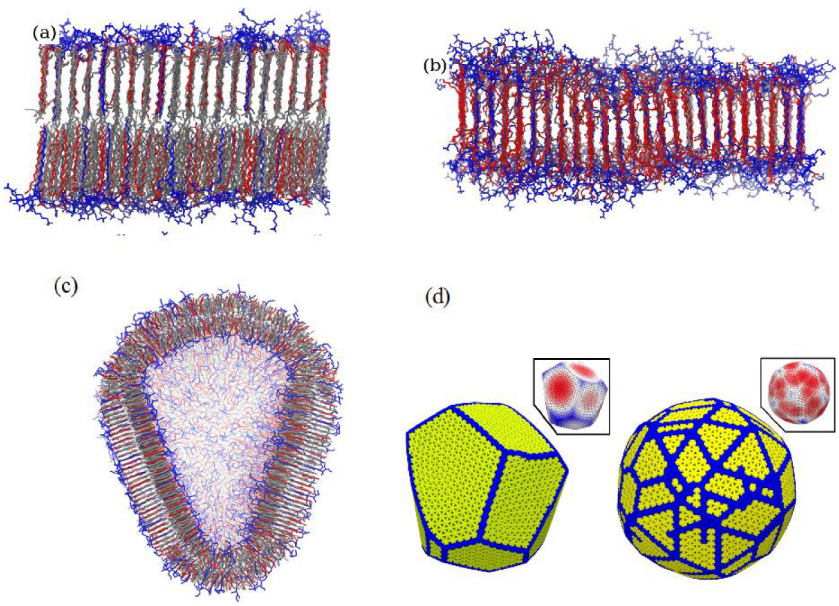

FIG. 2. Cationic and anionic amphiphiles design to co-assemble and organize into polyhedral shell shapes determined by a combination of WAXS-SAXS, TEM (not shown), full atom and coarse grained molecular dynamic (MD) simulations, and continuum elasticity. Bilayers at pH 4 (a) and at pH 8 (b) from full atom MD using the GROMACS 4.5.5 package. (c) Vesicles with shapes expected for heterogeneous elastic closed membranes at low pH values from coarse grained MD simulations using the MARTINI version 2.1 force field. (d) The continuum elastic model of mechanically heterogeneous shells (hard and soft components are shown in yellow and blue, respectively) shows that for fixed crystalline domain size, small vesicles (left: $\kappa_{hard}/\kappa_{soft} = 50$ for 95% of hard and 5% of components) have low symmetry shapes while large vesicles (right: $\kappa_{hard}/\kappa_{soft} = 20$ for 85% of hard and 15% of soft components) have more spherical shapes in agreement with TEM images.[4] Insets: vesicle height map with regions shown in red (blue) is closest (furthest) to (from) the center of the vesicle; the ratio of the largest (R_{max}) to the lowest (R_{min}) radius is $R_{max}/R_{min} \approx 1.1$. WAXS shows that the alkyl tails packing changes with pH from hexagonal (pH 4–7) to rectangular-C (pH 8–9.5) to hexagonal lattices (pH 10 and above). Adapted with permission from Leung *et al.*, ACS Nano **6**(12), 10901 (2012). Copyright 2012 American Chemical Society.

one +3 and three −1 chains into a four-tail bundle is then $E_e \approx 3(-1)l_B k_B T/d \approx -9k_B T$, where we have used the tail inter-chain distance observed by WAXS ($d \approx 0.5$ nm). This estimate is in agreement with the estimates from atomistic MD simulations of about $-2.8\ k_B T$ (30%) per NH_3^+–COO^- ion pair for their cohesive energy.[4] Adding the hydrophobic attraction from atomistic MD simulations, $-20k_B T$/chain, gives $E_b \approx -90k_B T$. In contrast to ionic driven assembly of incompatible molecules[20] and of molecules without reinforced attractions,[21] the ionic driven assembly discussed here induced short-range attractions among dissimilar molecules of opposite charge, explaining the observed stability of the ionic crystalline bilayer with the addition of salt up to salt concentration n = 500 mM NaCl.

In order to reveal the structure of the faceted vesicles at low pH, simulations with a MARTINI coarse-grained MD model[22] were also performed. In Figure 2(c), a MARTINI MD simulation snapshot shows that the internal structure of the bilayer in the vesicle is not homogenous. The vesicle can be thought of as a two-component shell, where one component represents the crystalline domains at the vesicle faces and the second component represents the liquid-like boundaries between the hard facets where the curvature is large.[4] The bilayer packing and thickness in the flat areas are in agreement with the full atom MD simulations (see Figure 2(a)).

Given that the size of the crystalline domains obtained by SAXS is about 30×30 nm,[2] the small vesicles of 100 nm to 200 nm in diameter have only few crystalline domains covering their surfaces. Therefore, these are more likely to be faceted into polyhedral structures with low symmetry; meanwhile large vesicles have nearly spherical faceted shapes. Both the small highly asymmetric and the large nearly spherical vesicles that were observed by TEM were recovered by the two-component elastic model (see Figure 2(d)). The crystalline domains of the vesicle faces represent the hard component with a bending modulus κ_{hard}, and the second (soft) component models boundaries between the hard facets, which are thinner and softer with a bending modulus κ_{soft}. The shapes in Figure 2(d) show vesicle shapes obtained by simulated annealing Monte Carlo optimization of a discrete triangulation[5] for large and small crystalline domains sizes, respectively ($Y_{hard}/Y_{soft} = 1$ since the Young modulus is less sensitive to thickness variations than the bending rigidity[23] and a related model of mechanically heterogeneous elastic shells[24] with $Y_{hard}/Y_{soft} > 1$ gives similar results). We note that if the edges of the polyhedra are liquid-like,[25] the shapes are not likely to change if the fraction of fluid to crystalline phases is low. Interestingly, the phase diagram for tail packing, as observed in Langmuir films,[24,26] allows fluid-hexagonal coexistence. However, there does not exist an obvious coexistence region between rectangular-C and fluid phases in monolayers, which may explain why the vesicles are only observed at the pH values when the tails are crystallized in a hexagonal lattice and are not stable at pH is 8 when the tails crystalline structure is rectangular-C.

Interestingly, the MARTINI MD simulations show disordered regions with high mean curvatures as predicted by the continuum model of heterogeneous elastic shells, even though these liquid-like regions have very low or null young moduli (Fig. 3). However, since the Gauss-Bonnet analysis only requires large bending rigidity differences (not Young modulus differences), the fragmentation of shells should be observed in shells with liquid and solid domains, provided the fraction of surface area covered by the liquid-like regions is very small compared to the fraction of area covered by the crystalline regions such that these easy to bend regions can form ridges.

In conclusion, the low symmetry faceted shapes in co-assembled vesicles of oppositely charged single-tail amphiphiles arise due to crystalline domains induced by ionic correlations among the headgroups and van der Waals interactions between the tails. These ionic correlations, as in ionic bonding, are not screened even at high salt concentrations generating membranes stable up to 500 mM of NaCl. Their crystalline lattice and morphology, however, are determined by the solution pH. The observed irregular faceted shapes arise only in hexagonal crystalline lattices, where crystalline domains are separated by soft interfaces that bend to release stress. Since ionic crystalline domains also arise upon the adsorption of multivalent ions on lipids,[27] our results suggest that spherical-to-faceted reversible transitions can be induced in cationic lipid vesicles by adding (or chelating) metallic multivalent ions.

In the present study, we found that for crystalline domains of the same sizes, small vesicles are more likely to be faceted into polyhedral structures with low symmetry (lower than the icosahedra)

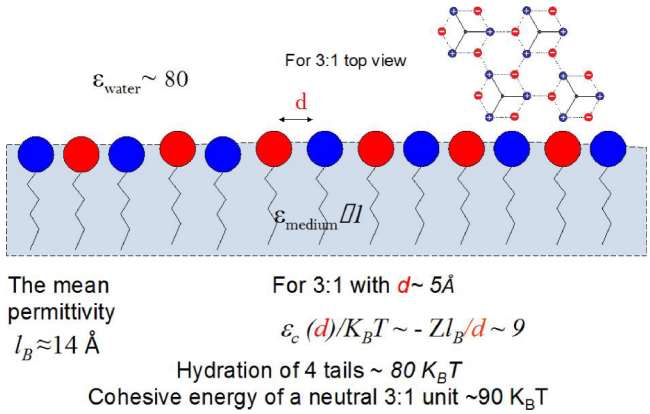

FIG. 3. Schematic of the cross-sectional area and top view of the co-assembled amphiphiles configuration that leads to the tail crystallization using the parameters from the x-ray experiments and estimates from the full atom simulations; here, ε_c is the electrostatic energy of a neutral 3:1 unit.

and large vesicles in which defects spread over many boundaries have nearly spherical faceted shapes. The kinetic path for the assembly of these faceted polyhedral vesicles may resemble the initial kinetic path observed in the formation of liquid vesicle where disk-like intermediate micelles are observed.[28] In the electrostatic driven co-assembly case, however, crystalline bilayers of various shapes may develop initially that subsequently merge into closed structures.

This combined theoretical, numerical, and experimental work explains the relation of the crystalline structure of the membrane to their geometries and elucidates the role of ionic interactions in the assemblies. The closed shells are shown to be stable only when the membrane crystal symmetry is hexagonal. This discovery will help researches to design shells in various geometries and elucidates the mechanisms used in nature to self-assemble cellular microcompartments and the shapes of halophilic organisms. For example, the robust envelope of Walby's rectangular bacterium takes a square geometry in natural brines, even though the cell wall is actually composed of a hexagonal lattice[29] of various lipids.

In summary, we have described the mechanism that connects the mesoscale structure of a complex system to the molecular scale conformation of the components. We exploited such connections to design a family of polyhedral shells. The elements required in the design involved geometric principles, elasticity theory, computer simulations, and experimental results. This example demonstrates that robust multicomponent structures can be assembled when ionic correlations reinforce molecular interactions at the nanoscale such as the packing of hydrophobic tails into crystalline lattice. In this case, the ionic assemblies are stable at high salt concentrations since the assemblies are self-screened. The mesoscale structure is a direct consequence of the constraints imposed by the geometrical packing.

This work was funded by the Office of Basic Energy Sciences within Department of Energy Grant No. DE-FG02-08ER46539. The computational work was funded by the Office of the Director of Defense Research and Engineering and the Air Force Office of Scientific Research under Award No. FA9550-10-1-0167 and performed by G. Vernizzi, R. Sknepnek, and B. Qiao. I thank M. J. Bedzyk, S. Kewalramani, and C.-Y. Leung for the SAXS-WAXS work and S. I. Stupp, M. A. Greenfield, C. J. Newcomb, and L. C. Palmer for the synthesis and TEM work.

[1] D. L. D. Caspar and A. Klug, Cold Spring Harbor Symp. Quant. Biol. **27**, 1 (1962).
[2] H. W. Kroto, J. R. Heath, S. C. Obrien, R. F. Curl, and R. E. Smalley, Nature **318**(6042), 162 (1985).
[3] S. Q. Cheng, Y. Liu, C. S. Crowley, T. O. Yeates, and T. A. Bobik, Bioessays **30**(11-12), 1084 (2008); C. V. Iancu, D. M. Morris, Z. C. Dou, S. Heinhorst, G. C. Cannon, and G. J. Jensen, J. Mol. Biol. **396**(1), 105 (2010); S. Tanaka, M. R. Sawaya, and T. O. Yeates, Science **327**(5961), 81 (2010).
[4] C. Y. Leung, L. C. Palmer, B. F. Qiao, S. Kewalramani, R. Sknepnek, C. J. Newcomb, M. A. Greenfield, G. Vernizzi, S. I. Stupp, M. J. Bedzyk, and M. O. de la Cruz, ACS Nano **6**(12), 10901 (2012).
[5] G. Vernizzi, R. Sknepnek, and M. O. de la Cruz, Proc. Natl. Acad. Sci. U. S. A. **108**(11), 4292 (2011).
[6] H. S. Seung and D. R. Nelson, Phys. Rev. A **38**(2), 1005 (1988).

[7] J. Lidmar, L. Mirny, and D. R. Nelson, Phys. Rev. E **68**(5), 051910 (2003).
[8] R. Zandi, D. Reguera, R. F. Bruinsma, W. M. Gelbart, and J. Rudnick, Proc. Natl. Acad. Sci. U. S. A. **101**(44), 15556 (2004).
[9] D. R. Nelson, *Statistical Mechanics of Membranes and Surfaces* (World Scientific, 2012), p. 1.
[10] R. Sknepnek, G. Vernizzi, and M. O. de la Cruz, Soft Matter **8**(3), 636 (2012).
[11] T. A. Witten, Rev. Mod. Phys. **79**(2), 643 (2007).
[12] A. E. Lobkovsky and T. A. Witten, Phys. Rev. E **55**(2), 1577 (1997).
[13] C. A. Haselwandter and R. Phillips, Phys. Rev. Lett. **105**(22), 228101 (2010).
[14] M. Dubois, V. Lizunov, A. Meister, T. Gulik-Krzywicki, J. M. Verbavatz, E. Perez, J. Zimmerberg, and T. Zemb, Proc. Natl. Acad. Sci. U. S. A. **101**(42), 15082 (2004).
[15] M. Dubois, B. Deme, T. Gulik-Krzywicki, J. C. Dedieu, C. Vautrin, S. Desert, E. Perez, and T. Zemb, Nature **411**(6838), 672 (2001).
[16] M. A. Greenfield, L. C. Palmer, G. Vernizzi, M. O. de la Cruz, and S. I. Stupp, J. Am. Chem. Soc. **131**(34), 12030 (2009).
[17] A. E. Walsby, Nature **283**(5742), 69 (1980); S. Nakamura, R. Aono, S. Mizutani, T. Takashina, W. D. Grant, and K. Horikoshi, Biosci., Biotechnol., Biochem. **56**(6), 996 (1992).
[18] R. R. Netz, J. Phys.: Condens. Matter **15**(1), S239 (2003).
[19] M. Tagliazucchi, M. O. de la Cruz, and I. Szleifer, Proc. Natl. Acad. Sci. U. S. A. **107**(12), 5300 (2010).
[20] F. J. Solis, S. I. Stupp, and M. O. de la Cruz, J. Chem. Phys. **122**(5), 054905 (2005).
[21] V. A. Bloomfield, Curr. Opin. Struct. Biol. **6**(3), 334 (1996); G. C. L. Wong and L. Pollack, Annu. Rev. Phys. Chem. **61**, 171 (2010); E. Raspaud, M. O. de la Cruz, J. L. Sikorav, and F. Livolant, Biophys. J. **74**(1), 381 (1998).
[22] L. Monticelli, S. K. Kandasamy, X. Periole, R. G. Larson, D. P. Tieleman, and S. J. Marrink, J. Chem. Theory Comput. **4**(5), 819 (2008); S. J. Marrink, A. H. de Vries, and A. E. Mark, J. Phys. Chem. B **108**(2), 750 (2004).
[23] W. T. Koiter, Proc. K. Ned. Akad. Wet., Ser. B: Phys. Sci. **73**(3), 169 (1970).
[24] R. Sknepnek and M. O. de la Cruz, Phys. Rev. E **85**(5), 050501 (2012).
[25] M. F. Demers, R. Sknepnek, and M. O. de la Cruz, Phys. Rev. E **86**(2), 021504 (2012).
[26] V. M. Kaganer, H. Mohwald, and P. Dutta, Rev. Mod. Phys. **71**(3), 779 (1999).
[27] B. F. Qiao and M. O. de la Cruz, J. Phys. Chem. B **117**(17), 5073 (2013).
[28] J. Leng, S. U. Egelhaaf, and M. E. Cates, Biophys. J. **85**(3), 1624 (2003).
[29] W. Stoeckenius, J. Bacteriol. **148**(1), 352 (1981).